# Light in the Cave: Opal coating detection by UV-light illumination and fluorescence in a rock art context. Methodological development and application in Points Cave (Gard, France)

Marine Quiers, Claire Chanteraud, Andréa Maris-Froelich, Emilie Chalmin, Stéphane Jaillet, Camille Noûs, Sébastien Pairis, Yves Perrette, Hélène Salomon, Julien Monney

# Light in the Cave: Opal coating detection by UV-light illumination and fluorescence in a rock art context

## Methodological development and application in Points Cave (Gard, France)

*Marine Quiers [a,*], Claire Chanteraud [b,c], Andréa Maris-Froelich [a], Émilie Chalmin-Aljanabi [c], Stéphane Jaillet [c], Camille Noûs [e], Sébastien Pairis [d], Yves Perrette [c,b], Hélène Salomon [c], Julien Monney [c]*

[a]*Laboratoire Commun SpecSolE, Envisol – CNRS - Univ. Savoie Mont Blanc, Chambéry, 73000, France*
[b]*Missouri University Research reactor - University of Missouri 65203 Columbia MO*
[c]*EDYTEM UMR5204, CNRS, Univ. Savoie Mont Blanc, Chambéry, 73000, France*
[d]*Univ. Grenoble Alpes, CNRS, Grenoble INP, Institut Néel, Grenoble, 38000, France*
[e]*Laboratoire Cogitamus, 1 ¾ rue Descartes, Paris, 75005, France*

** Corresponding author: m.quiers@envisol.fr*

**Abstract**

Silica coatings developed on rock art walls in Points Cave question the access to pictorial matter specificities (geochemistry and petrography) and the rock art conservation state in the context of pigment studies. However, classical *in situ* spectroscopic techniques appear unsuccessful to identify these coatings, which also prevent pigment characterization. In this study, we propose using a UV fluorescence method for opal coating detection based on the fluorescence specificities of uranyl-silica complexes composing these deposits. A coupling of spectral identification using UV laser-induced fluorescence spectroscopy with UV illumination was performed on samples and µ-samples from the Points Cave rock art site. The well-defined peaks observed in fluorescence emission spectra due to uranyl ions validate opal detection and its correspondence with green fluorescence observed under UV light at micro- and macroscopic scales. *In situ* optical measurements under UV illumination reveal the presence of opal coating, especially on rock art walls in Points Cave. Opal occurrence and repartition observations provide the first insights into Points Cave wall evolution and chronological constraints linked to opal coating development. Regarding the strong interactions with pigment suggested by

multiscale observations of samples and µ-samples, the impact of the presence of opal coating on Points Cave rock art conservation quality is questioned. Thus, by developing a specific and non-destructive characterization method for opal coatings, this study opens up a new approach for the study of decorated wall taphonomy and proposes utilizing mineralization both as markers of the natural history of caves and as an indication for their occupation by ancient human groups.

**Keywords**: Silica coating, uranyl, UV fluorescence, *in situ* detection, rock art cave, Quaternary, archaeology, Ardèche, France, optical methods

## 1. Introduction

Natural activity in caves, mostly weathering, transforms the physical, chemical and mechanical conditions on the surface of the walls (Bassel, 2017; Chalmin *et al.*, 2018). Thus, the traces of all these transformations (environmental input) can be a source of information regarding natural and anthropological events on the wall surface, such as drawing and painting realizations, cave environment evolution, and human attendance in the cave (Sadier, 2013; Pons-Branchu *et al.*, 2014; Quilès *et al.*, 2015; Quing-Feng *et al.*, 2017; Garate *et al.* 2018; Valladas *et al.*, 2017; Money & Jaillet, 2019).

Among the taphonomic processes impacting rock art pictorial matter, mineral-coating formation as weathering products is well described in rock art research (Huntley, 2012). Silica rich amorphous deposits, also called silica skins, have been observed at different cave and open-air parietal sites (Watchman, 1990; Aubert *et al.*, 2004; Aubert *et al.*, 2012; Huntley, 2012). Thus, studies have suggested both a positive and negative impact on rock art conservation due to opal coating

development. Indeed, the strong interaction suspected with haematite pigments has been suggested as an element of conservation enhancement, notably compared with other pigments (Watchman, 1990). However, some authors have also observed exfoliation processes of silica skins, which could play a role in rock art weathering (Aubert *et al.*, 2004; Green *et al.*, 2017). To our knowledge, there is still no clear answer on the role of silica coatings as conservation factors of pictorial matter. In addition to this conservation issue, silica skins have been proposed as tools for indirect dating of parietal art, especially in the case of inorganic pictorial matter (Aubert *et al.*, 2004; Aubert *et al.*, 2012). Indeed, this mineral phase is known to be enriched in uranyl ions, but the U-Th dating application remains hypothetical due to silica skin thickness and absence of stratigraphy, which complicate both sampling and measurement reliability (Green *et al.*, 2017).

Thus, even if silica skin characterization represents a key issue in the rock art context, it remains difficult to identify and characterize, especially with non-invasive techniques. Currently, the use of *in situ* spectroscopic techniques in rock art studies is increasing, as these methods can provide information on both pictorial matter and pigment environments (substrate, deposits, concretions, etc.). The portability and decreasing cost of instruments coupled with the rapidity and the non-destructive character of analyses have led to a quasi-systematic use of these techniques in recent rock art studies (Huntley, 2012). However, amorphous silica characterization, even in the rock art context, is generally based on laboratory observations such as SEM or XRD analyses (Watchman, 1990; Gaillou *et al.*, 2008; Garcia-Guinea *et al.*, 2013; Huntley *et al.*, 2015; Green *et al.*, 2017). In addition, the signal of pictorial matter acquired with portable spectroscopic techniques could be impacted by the presence of silica skins, as observed by Huntley (2012) in the case of pXRF measurements.

In this paper, we propose a new method for the *in situ* detection and characterization of amorphous silica in a rock art context based on UV laser-induced fluorescence (LIF). Indeed, uranyl fluorescence characteristics under UV light are well known and have been observed in silica mineralization, especially in opal (deNeufville *et al.*, 1981; Gorobets *et al.*, 1977; Fritsch *et al.*, 2001; Gaillou *et al.*,

2008). Thus, UV spectroscopy presents the same advantages as other portable spectroscopic techniques, but the bright green fluorescence and the specific spectral features displayed by uranyl ions enable the targeted identification of opal coatings. To our knowledge, only one study has reported opal detection in caves using optical methods based on UV techniques (Garcia-Guinea *et al.*, 2013), and no study has applied UV spectroscopic methods in a rock art context for opal identification. Here, we propose a methodological development based on laboratory and field experiments to validate the use of *in situ* UV techniques for opal detection in a rock art context by coupling *in situ* optical and spectroscopic analyses to obtain multiscale information.

This study was performed in Points Cave (Aiguèze, Gard, France), which contains an important spread of opal coating on the cave walls. In this approach, Points Cave perfectly illustrates the importance of environmental input characterization in the study of rock art. The advantage of this site is given by the presence of colouring flakes falling from cave walls, allowing transport, µ-sampling and analysis in the laboratory. Analysis of these coloured flakes allows us to identify and measure the environmental input, which modifies and obscures the identification of pictorial matter characteristics.

## 2. Material

### 2.1 Study site: Points Cave

Located in the Ardèche River gorge less than 10 km downstream of Chauvet Cave, Points Cave is a Palaeolithic rock art site identified in 1993 (Figure 1) (Deschamps *et al.*, 2018). Archaeological studies have been performed since 2011 as part of the "Datation Grotte Ornées" project ("Cave Art Dating" project, Monney, 2011; 2018). The entrance opens on a hundred-metre long gallery in Urgonian limestone. Rock art, exclusively composed of red imprints, is present in a unique sector in the middle part of the gallery, preserved from sunlight. Excavations conducted at the entrance indicated human and animal occupation during the Upper Palaeolithic (Monney & Jaillet, 2019).

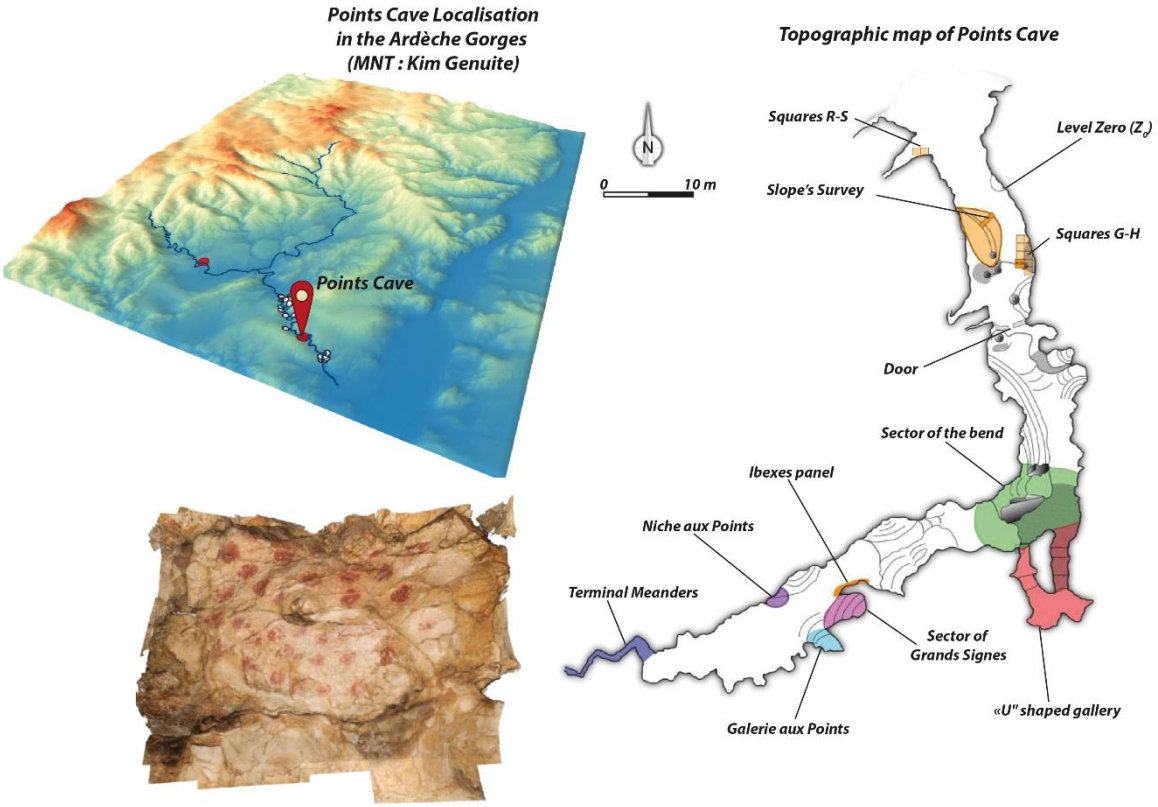


***Figure 1**: Points Cave location in southeastern France and topographic map; photography of graphic entities: "Niche aux Points".*

Points Cave is currently disconnected from hydrogeological flows (Jaillet & Monney, 2018). Only a few infiltrations can be observed after strong precipitation events. The low level of leaching on the wall and the quasi-absence of a calcite veil are due to this weak hydrogeological activity. Millimetric to centimetric concretions and efflorescences (coralloid type of crystallization) have developed on the wall surface in the decorated sector.

### 2.2 Points Cave pictorial matter

Parietal ornamentation, composed exclusively of reddish tracings and paintings, is currently observed in the middle part of the gallery. It comprises 59 palm-printed dots, commonly referred to as "palm points". This ornamentation also consists of five animal representations (three ibexes, a horse and a bison), two bilobed signs, an angular line and a few indeterminate traces (isolated lines and dots) (Monney, 2018). Moreover, archaeological colouring matter has been found in this sedimentary sequence at the entrance of the cave (Chanteraud & al., 2019; Chanteraud, 2020).

Investigations carried out at the foot of the rock art panel known as the "Great Signs" found five coloured wall flakes: S-ECA-01 to S-ECA-05 (Figure 2). Composed of limestone detached from the wall under mechanical action, these 3 to 20 cm flakes are covered on one side with colouring matter, probably coming from the large bilobed sign (graphic entity PTS-10) or from other unknown rock art panels that may have crumbled entirely from the walls nearby. These flakes are a major asset of Points Cave because they allowed us actual fragments of the decorated wall and transport them to the laboratory.

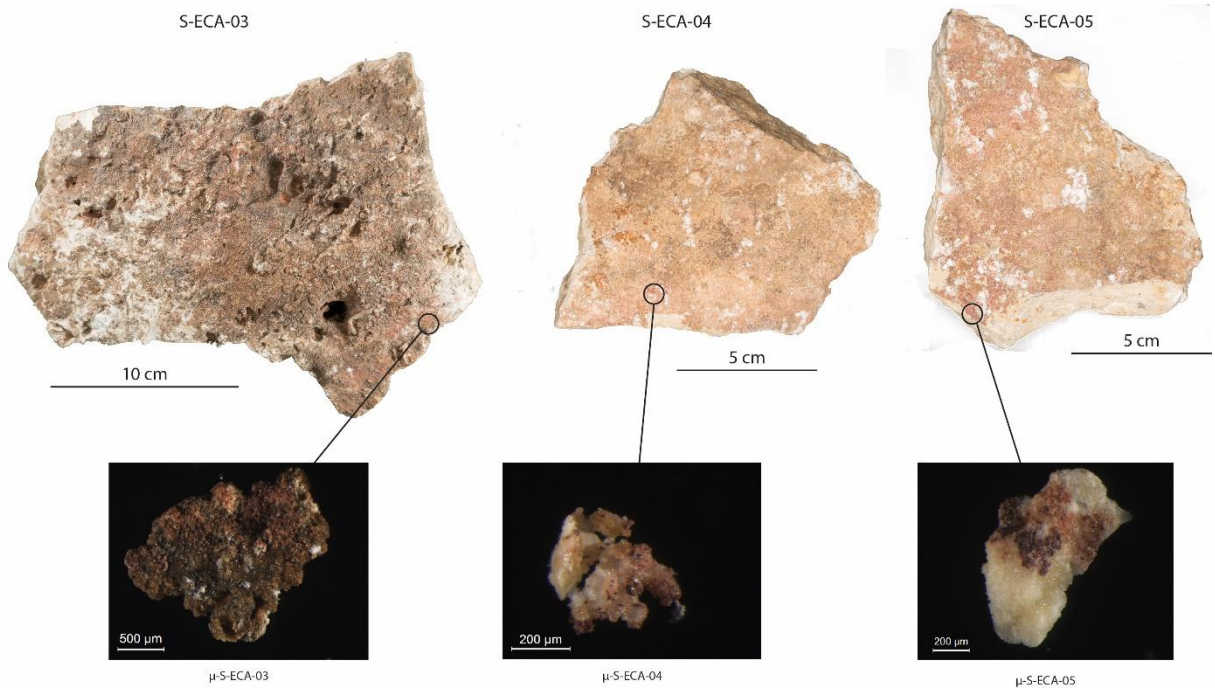


***Figure 2****: Limestone flakes found at the foot of the Bilobed Signs panel, location of µ-sampling.*

To identify both the iron-oxide morphologies and the natural mineralization that can form on the surface of the decorated walls, our study was centred around the five wall flakes discovered in the decorated sector of Points Cave and the 20 µ-samples taking from the decorated panels of the cave. One µ-sample of pictorial matter was performed on each coloured flake (µS-ECA-01 to µS-ECA-05). All µ-samples were observed and analysed without any preparation (Figure 2).

## 3. Methods

### 3.1 Macroscopic and microscopic observations

#### *3.1.1 Laboratory and in situ observations at macroscopic scale*

Image capture for macroscopic observations was performed in two steps: 1) a photograph was taken

under white light, and 2) another photograph was taken under UV light illumination. Observations at the macroscopic scale in the laboratory and in the cave were realized with a Canon EOS 5D Mark III camera and a Canon EOS 7D camera fixed on a tripod. A detached flash was used for image capture under white light. For UV light illumination, 4 UV LEDs (280 nm, 2.26 W, NewEnergy) were fixed on orientable macroflash bars on each side (2 LEDs per side) of the camera, allowing both macrophotography and general views of cave walls. Camera parameters are available in Table 1.

***Table 1****: Camera parameters used for both white and UV light illumination during field and laboratory macroscopic observations.*

| | | | *Aperture* | *Obturation speed (sec)* | *Iso* |
|---|---|---|---|---|---|
| **Laboratory** | White light | | F/7.1 | 1/320 | 1600 |
| | UV light | | F/7.1 | 10 | 1600 |
| **Field** | White light | *Macro* | F/11 | ½ | 320 |
| | | *Wall view* | F/11 | 1/60 | 100 |
| | UV light | *Macro* | F/4.5 | ½ | 320 |
| | | *Wall view* | F/11 | 15 | 320 |

Laboratory observations were also performed using a stereomicroscope (LEICA M165 C) under white and UV light. The same 4 LEDs were used for UV illumination.

### 3.1.2 Laboratory observations at the microscopic scale

At the microscopic scale, observations of µ-samples of flakes on carbon tape were realized with a field-emission scanning electronic microscope (SEM) ZEISS Ultra+ associated with an EDX (energy

dispersive X-ray) probe (SDD, Bruker) working in high-vacuum mode with a 15 keV voltage. Images were taken with secondary electrons using in-lens or Everhart-Thornley detectors (SE2) and with backscatter electrons (BSE-AsB detector) (Néel Institut, Grenoble).

### 3.2 UV fluorescence analyses

Stationary fluorescence signal of flake and flake µ-samples was measured in the laboratory with a solid-phase spectrofluorimeter designed in the EDYTEM laboratory for non-destructive solid-phase measurements (Perrette *et al.*, 2000).

This instrument is divided into excitation and detection compartments associated with a translation stage system for sample surface measurement. For this experiment, the excitation system was composed of a Nd:YAG laser (Crylas, FQSS266-Q1) with a 266 nm excitation wavelength. The fluorescence emission response was collected after sample excitation by focusing the laser beam (~30 µm) on its surface. The detection system was composed of a low-pass filter monochromator (Jobin Yvon, MicroHr) for light diffraction, fitted with a 300-g/mm diffraction-grating centred at 620 nm, associated with a thermoelectric-cooled, back-illuminated CCD (Jobin Yvon, Sincerity) for high-efficiency signal detection in the UV-visible light domain. As no manipulation, modification or destruction of the sample surface occurred during analysis, this technique is suitable for archaeological sample measurements.

Two types of fluorescence measurements were realized:

- Single point measurements were performed on flake µ-samples (µS-ECA-03, µS-ECA-04 and µS-ECA-05). One spectrum was independently acquired on the sample. Measurement location was determined manually. An acquisition time of 1 s and a monochromator entrance slit of 0.25 mm (~1 nm spectral resolution) were used for spot spectrum acquisition.
- Surface measurement was performed on flake S-ECA-05. The motorized translation stage

system allowed movements in two directions for surface measurements. The image was obtained by stacking lines along the Y-axis. For this study, fluorescence surface imaging was performed with a 100×100 µm resolution using a 0.1 s acquisition time and a 0.05 mm entrance slit.

Data pre-processing was performed with MATLAB software. Spectra were corrected from baseline and instrument responses and then filtered with the Savitsky-Golay method (Savitzky & Golay 1964).

## 4. Results

### *4.1 Macroscopic scale observations*

At the macroscopic scale, no mineralization was observed on the walls, flakes or µ-sample surfaces. Here, the coralloid type of crystallization was not taken into account due to its centimetric size. In fact, at this observation scale, surfaces seemed to be well preserved with strong colouration from the pictorial matter and clear access to the calcareous substrate (Figure 2).

It has been shown that decorated panels of the cave display various mineralizations, such as calcium sulphate (Chanteraud *et al.*, 2020). However, these deposits remain invisible even after inspection under a stereomicroscope, revealing the need for microscopic inspection using SEM.

### *4.2 Microscopic scale observations*

At the microscopic scale, a 1 µm-thin mineral film consisting of nonordered spheres was identified as silica mineralization on flake µ-samples (Figure 3). Its geochemistry and hummocky morphology are

related to a type A-g amorphous opal with a $SiO_2nH_2O$ formula (Flörke *et al.*, 1991). The mineral structure present on coloured flakes suggested its formation from a water film containing a high concentration of silica (Monger and Kelly, 2002; Curtis *et al.*, 2019).

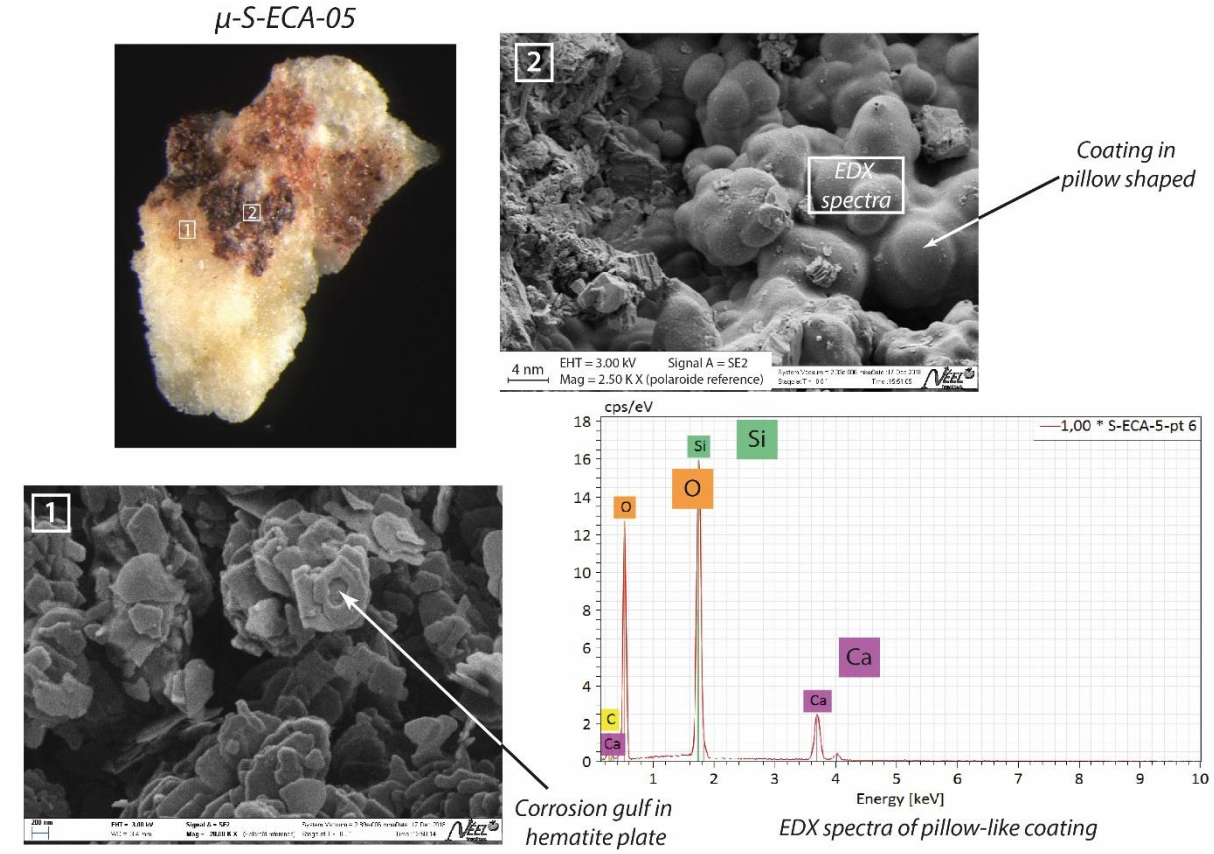


***Figure 3**:* SEM observations of µ-S-ECA-05. 1/ Corrosion gulf in hematite plate observation in Secondary Electron mode (SE); 2/ Pillow-like silica coating on surface in SE mode; White rectangle = Area of EDX spectra on the pillow-like silica coating.

Concerning the µ-samples from the decorated walls, the same observations were noted, including pseudohexagonal platy haematite and some strong indications of opal. Importantly, these samples showed significant opal development, with a complete coating of the pictorial matter to the extent that the morphology of the haematite was no longer observable on the surface.

SEM observations of flake µ-samples allowed us to identify pictorial matter as haematite due to its colour and macro- and micromorphologies. Typically, the haematite composing the pictorial matter was pseudohexagonal and showed corrosion gulfs (Figure 3). Weathered haematite plates seem to have been "ingested" by the silicate coating and could only be observed when a section was accessible on the surface of the sample (Figure 4). However, preliminary studies on the walls of Points Cave using portable spectroscopic techniques (pXRF and Raman) could not identify the presence of opal coating *in situ* (Chanteraud *et al.*, 2020).

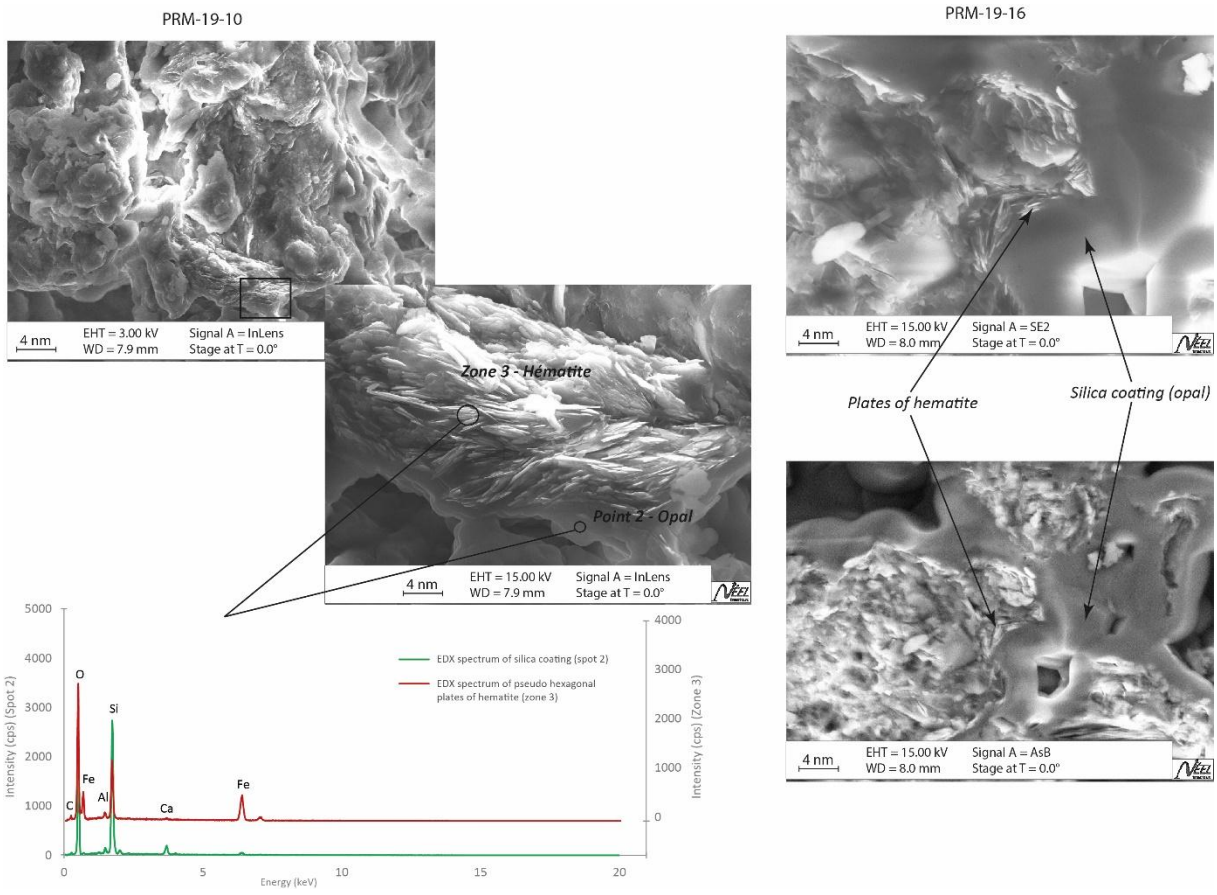


***Figure 4**: Haematite plates embedded in the opal coating on PRM-19-10 and PRM-19-16 µ-samples (SEM observation in SE and BSE mode).*

### *4.3 Opal identification by UV-fluorescence*

To evaluate the potential of UV fluorescence to detect the opal mineral phase, fluorescence analyses were first performed on 3 flake µ-samples (µS-ECA-03, µS-ECA-04 and µS-ECA-05) that were previously characterized by different geochemical analyses. Due to the small size of the samples (approximately 200 µm), only a few localized spectra were recorded. The spectra obtained could be divided into different emission regions depending on the main signal sources (Figure 5):

- From 300 to 470 nm, this region corresponds to the fluorescence emission of the sample matrix. Peaks and shoulders were detected at approximately 350 nm, 380-390 nm, 410 nm and 430-440 nm. According to the literature, they could be associated with organic matter entrapped in the crystalline matrix (McGarry & Baker, 2000; Perrette *et al.*, 2000; Van Beynen *et al.*, 2001; Perrette *et al.*, 2005; Quiers *et al.*, 2015) or with the silica material fluorescence response to UV-light excitation (Boyko *et al.*, 2011; Garcia-Guinea *et al.*, 2013).

- From 470 to 750 nm, special features were identified in this part of the spectra for samples µS-ECA-04 and µS-ECA-05. They were characterized by a sequence of 3 defined peaks at 501, 521, and 545 nm and a shoulder at approximately 572 nm. These peaks were identical in all spectra measured on µ-samples µS-ECA-04 and µS-ECA-05 and coincided with the uranyl ion spectrum in silica matrices based on a review in the literature (Table 2).

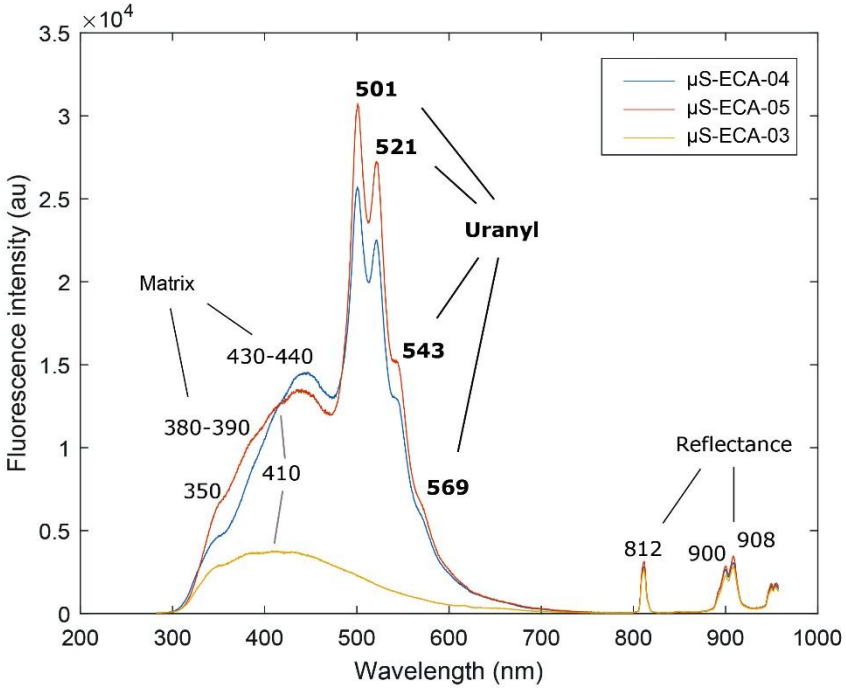


**Figure 5**: Mean fluorescence emission spectra (excitation 266 nm) of samples µS-ECA-04 (blue), µS-ECA-05 (red) and µS-ECA-03 (orange). Spectra are divided into three different regions as a function of the main fluorescence signal sources: sample matrix, uranyl ions and laser emission reflectance.

Entrapment of uranyl ions in siliceous matrices, especially opal phases, is well documented in the literature (Zielinski, 1980; Kasdan *et al.*, 1981; Kinnunen & Ikonen, 1991; Neymark *et al.*, 2000; Fritsch *et al.*, 2001; Gaillou *et al.*, 2008; Devès *et al.*, 2012; Fritsch *et al.*, 2015; Othmane *et al.*, 2016). The strong affinity of uranyl groups for amorphous silica leads to a strong U-opal association, which is stable at the scale of geological time (Othmane *et al.*, 2016). Thus, uranyl-specific spectra could be associated with the presence of opal on samples, and UV fluorescence analysis represents an efficient tool for its identification. As opal detection was subject to uranyl fluorescence properties, detection using UV fluorescence was dependent on uranium entrapment in silica crystalline structures. In their study of opal gems from different geographic and geological contexts, Gaillou *et al.* (2008) showed that not all opals are fluorescent. Opal fluorescence can be divided into two classes: blue fluorescence

caused by intrinsic oxygen-related defects typical of amorphous silica structures and green fluorescence attributed to uranyl groups (Fritsch *et al.*, 2001, 2003), which is believed to be typical of common opals. A low content of U (≥ 1 ppm) automatically induces a green fluorescence response to UV light excitation and can reach more than 100 ppm in some deposits (Gaillou *et al.*, 2008). Garcia-Guinea *et al.* (2013) measured a uranium amount of 193 ppm in stalactites in Castanar Cave. Thus, detection of opal via UV fluorescence is not systematic but common, as a low content of uranium allows fluorescence emission. However, uranium concentration in Points Cave µ-samples have not been measured due to the particularly thin opal layer and the impossibility of destroying µ-samples.

**Table 2**: Fluorescence emission peaks for different opal or amorphous silica deposits reviewed in the literature.

| | **Fluorescence emission peaks (nm)** | | | | |
|---|---|---|---|---|---|
| Othmane *et al.* 2016 | 504 | 524 | 546 | 570 | - |
| | 504 | 523 | 545 | 573 | - |
| Fritsch *et al.* 2015 | 504 | 524 | 546 | 572 | 604 |
| Brennan & White 2013 | 502 | 520 | - | - | - |
| Garcia-Guinea *et al.* 2013 | 505 | 524 | 543 | 569 | 650 |
| ***This study*** | **501** | **521** | **545** | **572** | - |

To evaluate method accuracy at a larger scale, a second experiment was performed directly on flake S-ECA-05. UV fluorescence cartography (100 x 100 µm resolution) showed a range of spectra presenting uranyl spectral characteristics. Assuming that the fluorescence signal can be interpreted as a mixing of a uranyl signal with a matrix signal, opal information was extracted from fluorescence cartography using a mixing algorithm, MCR-ALS, with the MCR-ALS toolbox in MATLAB software

(Jaumot *et al.*, 2015). MCR-ALS has become a popular chemometric method in solving mixture analytical models. It is based on an additive bilinear model of pure contributions that depends on the concentration and the specific spectral sensitivity of each component. This algorithm can also be applied to obtain quantitative information (Jaumot *et al.*, 2005; de Juan *et al.*, 2014; Zhang & Tauler, 2013). A singular value decomposition (SVD) method was first used in the MCR calculation to define the number of initial loadings. Thus, three components were estimated that mainly contributed to the fluorescence signal. These three initial loadings were calculated using the PURE algorithm, a commonly used method to find the purest variable, and could be associated with uranyl fluorescence spectra, matrix fluorescence signal and background signal (Figure 6).

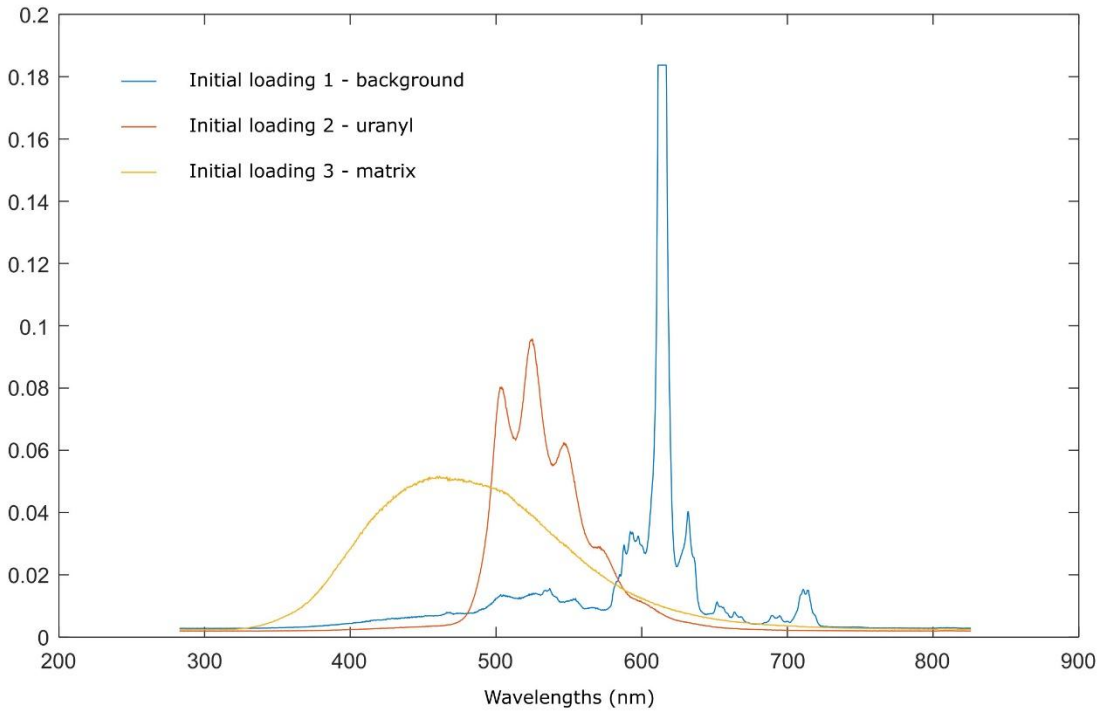


***Figure 6**: Initial loadings obtained with the PURE algorithm on fluorescence cartography spectra.*

MCR-ALS was then performed based on these 3 initial loadings. Non-negativity constraints were applied. Model results ($r^2$=99.88) indicated a contribution of uranyl to the sample fluorescence signal

321 and thus to a proportion of opal at the sample surface (Figure 7).

322

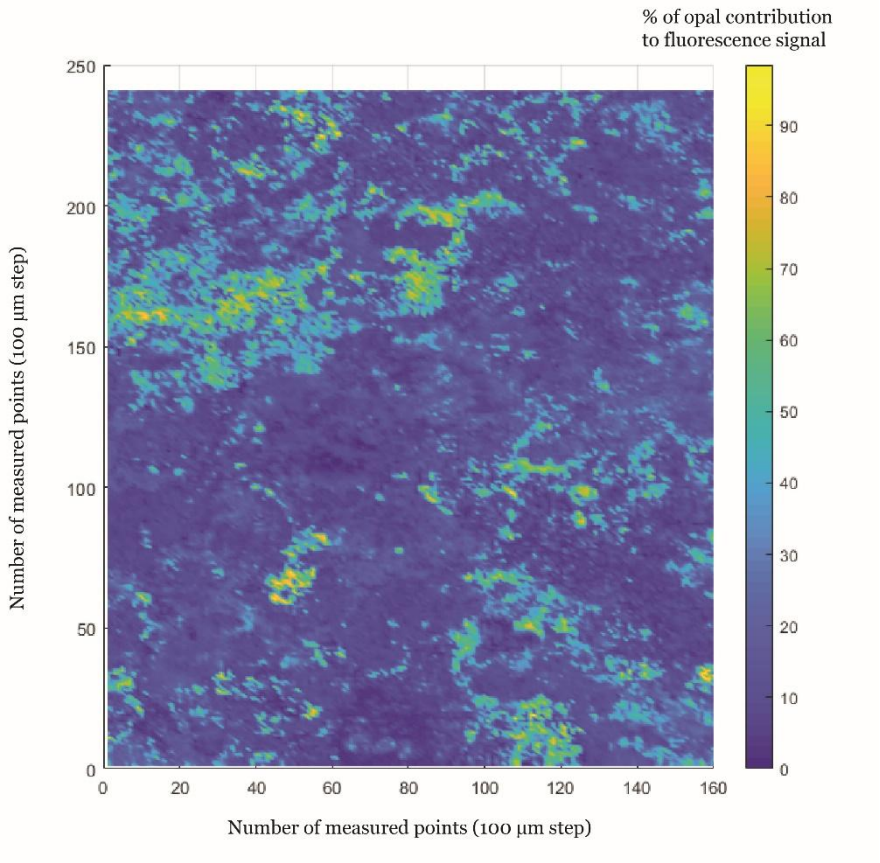


323

***Figure 7****: Opal fluorescence signal proportions measured on the S-ECA-05 flake and obtained with the MCR-ALS algorithm.*

324

325 Evaluation of opal proportions on the sample using this method is, however, subject to certain biases.
326 Similar to the majority of spectroscopic techniques, this detection method can only detect surface
327 deposits. Thus, opal mineralization located under other mineral or organic deposits cannot be detected.
328 Moreover, for quantitative measurement, the measurement sensitivity to changes in sample surface
329 microtopography must be taken into account. As the laser beam is focused on the surface, variations in
330 fluorescence intensities measured on the sample, and thus opal estimations, can be biased by
331 millimetric changes in surface relief.

In addition, this method remains effective in extracting information on opal mineralization even on heterogeneous matrices, such as the Points Cave µ-samples. Due to its specific spectral shape, uranyl signal can be easily extracted from mixed fluorescence signals. In addition, mixing algorithms could provide quantitative information if combined with calibration methods. Indeed, the MCR-ALS algorithm has been used for the quantification of different target molecules based on various spectroscopic data (Mas *et al.*, 2010; Araya *et al.*, 2017; Kumar *et al.*, 2018; Castro *et al.*, 2021). Regarding sample complexity, calibration protocols based on standard references and prepared or artificial mixtures are difficult to apply (Araya *et al.*, 2017). Quantification strategies need to be developed for archaeological materials, reaching a balance between sample destruction and model result robustness, such as those developed for hyperspectral data. Then, the estimated concentration accuracy will depend on the legitimacy of the assumption made in the quantification strategy (Araya *et al.*, 2017).

### *4.4 Visual detection under UV light: laboratory experiments*

As explained previously, minerals containing uranyl ions ($UO_2^{2+}$) have been known to exhibit strong fluorescence marked by specific spectral features and temporal characteristics since at least early 1900 (deNeufville *et al.*, 1981). The bright green fluorescence of uraniferous opal is a well-known characteristic of this mineral phase and has been related to the presence of uranium (Gorobets *et al.*, 1977; Fritsch *et al.*, 2001). To evaluate whether this specificity can be used for opal detection, flake µ-samples were exposed to UV light (see 3.1.1). The results show that µ-samples µS-ECA-04 and µS-ECA-05 exhibited a bright green-light response (Figure 8). These two sample spectra contained specific features corresponding to the fluorescence emission of uranyl ions. Green illumination was thus associated with the presence of U-opal on these samples. The case of µ-sample µS-ECA-03 was more complex. While the fluorescence spectrum did not show any spectral features associated with the uranyl signal, localized greenish fluorescence could be distinguished on the sample. This could be

359 explained by a less precise measurement due to a more difficult targeting of opal because of the higher
360 sample size or more scattered opal distribution. Second, the sample surface was more coloured and
361 had more pictorial matter (cf. §4.1), suggesting decreased ability for detection.
362

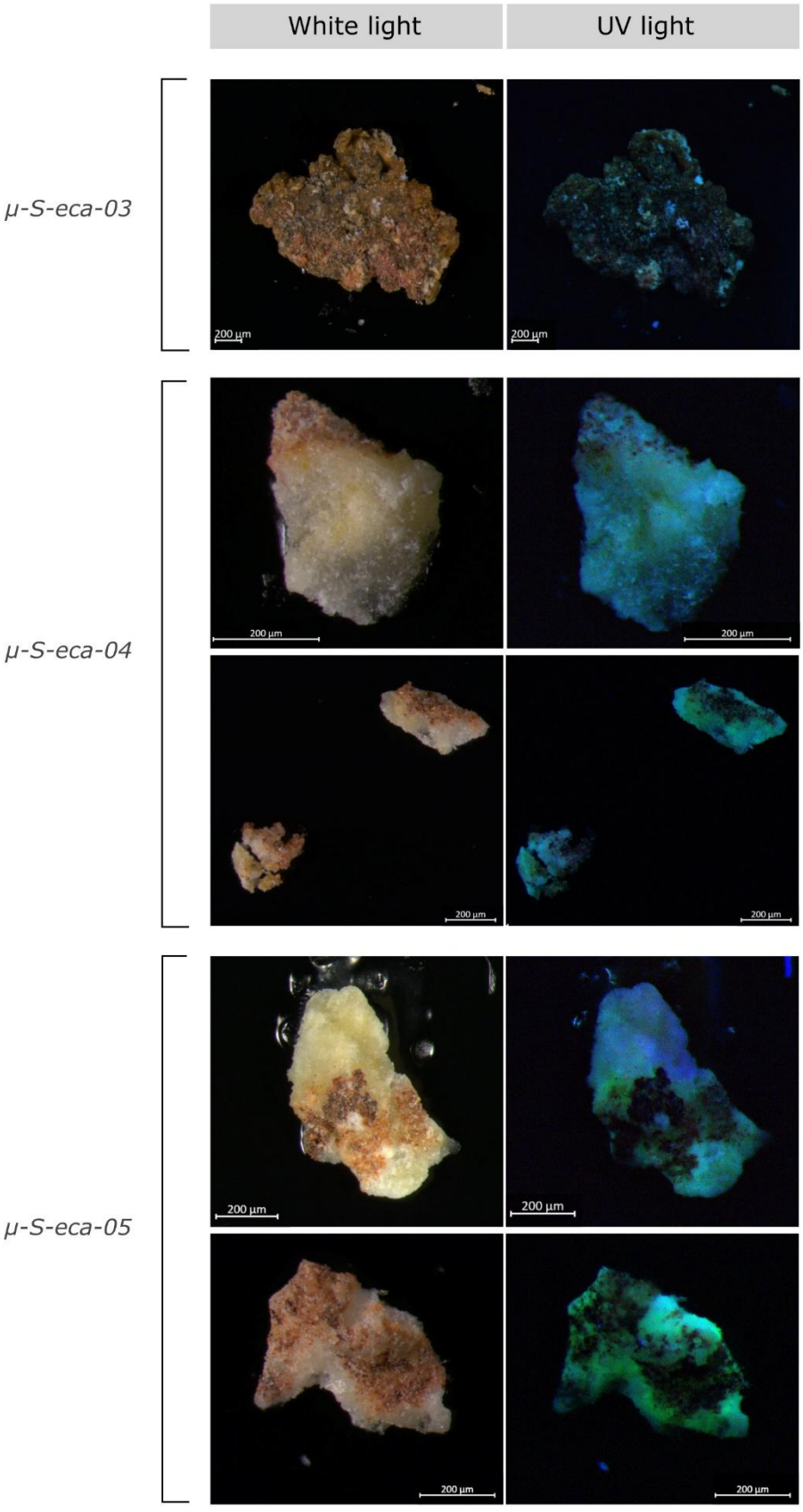


363

***Figure 8**: Photographs of three µ-samples taken on flakes under white and UV light.*

Considering that uranyl green illumination is representative of the presence of opal, detection concordance between spectral and visual techniques was tested at a larger scale by comparing UV-illuminated photographs with UV fluorescence cartography of flake S-ECA-05 (Figure 9). For this purpose, the green component of the RGB image was extracted from UV-light photos. The grayscale image was subtracted to avoid the luminosity effect, and a threshold was applied to the image obtained to select only pixels containing green colour. To help compare the opal information provided by both techniques, images were aligned using point control selection and geometric transformation functions in MATLAB.

The results show a high correspondence between spectral and visual detection methods. To evaluate the efficiency of the optical method, opal cartographies with different detection limits were simulated using the opal contribution percentage to the fluorescence signal from spectroscopic measurements and compared with optical data. The opal contribution threshold of 27% presented the best correlation coefficient with opal extracted from UV photographs ($R^2$=0.50). This indicated that opal detection with the optical method was efficient when opal fluorescence emission contributed at least 27% of the total fluorescence signal of the sample. Under this threshold, the detection efficiency decreased for the optical method. The rather low correlation coefficient between both images could mainly be explained by the point control selection and geometric transformation applied to readjust them together. Angle disposition of the sample and detector combined with image resolution could have led to difficulties in adjusting the images. Further research in the computational image domain could improve the methodology and enhance the correlation between the two techniques.

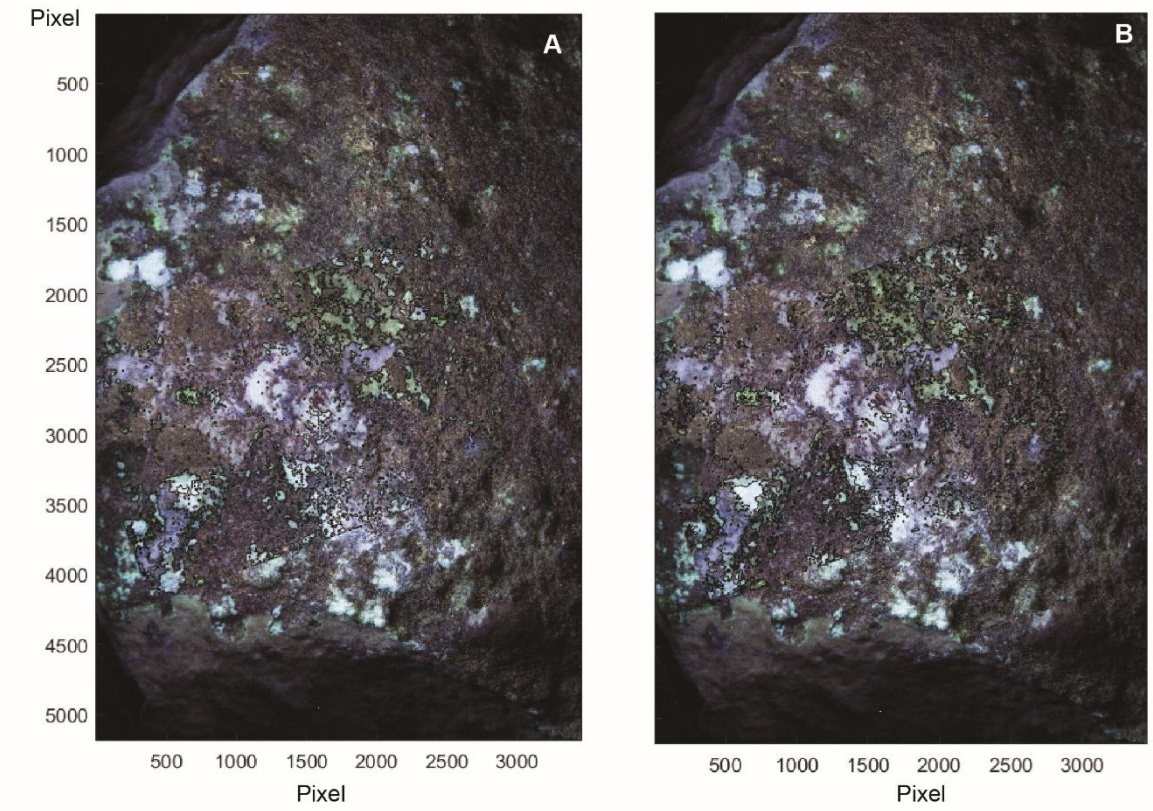


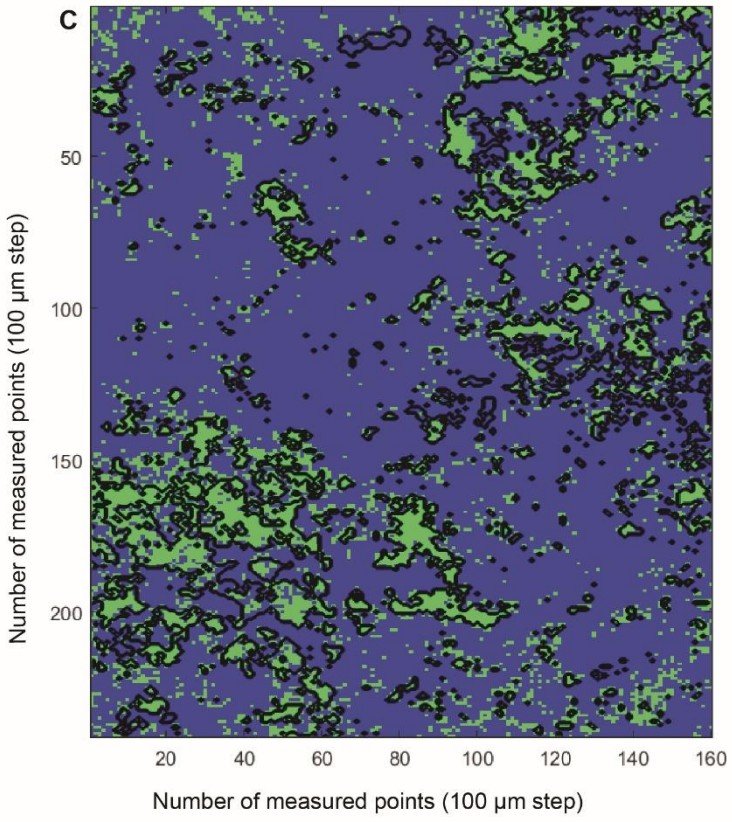


**A** - Photo under UV ligth with contour plot (black line) of opal location obtained by extraction of the green component of the image

**B** -Photo under UV ligth with contour plot (black line) of opal location obtained by MCR-ALS on fluorescence map

**C** - Opal location on sample obtained from fluorescence signal (green zones, 27% of signal contribution) and from UV photo (black lines)

387

***Figure 9****: Detection and location of opal mineralization on flake S-ECA-05 obtained using UV illumination (A) and UV fluorescence techniques (B).*

*The two methods are compared in C.*

388

389 *4.5 Visual detection under UV light: field experiments*

390

391 An *in situ* photographic protocol that alternated white light and UV illumination was applied to the
392 Points Cave walls. As shown in Figure 1, three rock art panels were investigated with one wall where
393 rock art was absent. Images were realized at both the wall and macroscopic scales.

394

395 At the wall scale, the rock art panels investigated (Niche aux Points, Bilobed Signs and Ibexes)
396 displayed large green fluorescent zones when illuminated by UV LEDs (Figure 10). This green
397 fluorescence response was consistent with preliminary results obtained in the laboratory on cave wall
398 flakes and µ-samples from these zones. Thus, UV illumination successfully enabled the detection of
399 opal coatings on these walls, according to the green response observed in photographs.

400

401 In contrast, no opal signal appeared clearly distinguishable in photographs of the wall situated a few
402 metres before the art panel. These photographs displayed greenish fluorescence mixed with other
403 signals, making it difficult to identify and extract green colour with accuracy. Spectroscopic
404 measurements need to be performed to precisely identify the presence of opal.

405

406 Macroscopic-scale observations under UV light allowed the targeting of specific deposits or zones on
407 cave walls. In the particular case of the Bilobed Signs panel, macroscopic investigation targeting
408 flaking zones revealed a contrast between the rock art panel and the zones where flakes had detached
409 from the wall. Indeed, the left part of the UV photograph (Figure 10) displayed numerous green
410 fluorescent spots, whereas they were absent from the right part of the photograph. Efflorescence

concretions on cave walls, which are widely spread in Points Cave, were also investigated, but the presence of opal has not yet been validated.

## 5. Discussion: Implications of opal detection for rock art studies at Points Cave

### 5.1 Contribution of UV fluorescence techniques

According to the first results obtained using the *in situ* UV illumination method and the preliminary results obtained in the laboratory on cave wall flakes and µ-samples from rock art panels, *in situ* measurements successfully detected the presence of opal in Points cave. Indeed, the green fluorescence observed on Niche aux Points, Bilobed Signs and Ibexes panels suggests that opal development covers a large area of cave walls, especially in rock art zones. Macroscopic observations also help to provide initial insights into rock art-opal interactions, as UV light allows for the targeting of specific deposits or zones on cave walls. It provides complementary information on opal distribution and interaction with archaeological material. For example, investigation of the flaking zone suggests a current absence of extended opal film or opal mineralization, probably due to desquamation occurring on this wall.

However, the opal signal is not always clearly distinguishable, as observed on the wall outside of the rock art zone or on coralloid concretions. Yet, these speleothems are known to contain a silica layer enriched with uranium (Monney *et al.*, 2019; Barbarand et Nouet, 2020). Alternating layers of silica and calcite or the presence of calcite cover could explain the ambiguous signal. First, this highlights the need for *in situ* fluorescence spectroscopic measurements to validate the photographic identification of the opal mineral phase in cases where the green response is not clearly detectable. Second, colour perception varies greatly from one image to another, even within the same site, making it difficult to evaluate the mineral phase distribution. Even if camera and image treatment parameters

437 influencing colour display (white balance, exposure time, filters, etc.) can be easily standardized,
438 lighting variations (LED orientation, position, distance from wall, etc.) are difficult to homogenize. As
439 this paper presents preliminary results attempting to validate the detection method, no protocol for
440 colour calibration was applied. Further research on the Points Cave site will be subject to the
441 development of a colour calibration procedure.
442
443 Finally, UV illumination also highlights various types of deposits, sometimes not clearly detected
444 under white light. After fluorescence analyses in the laboratory or directly *in situ*, this technique could
445 help to detect other mineral or organic phases. Moreover, it is interesting to note that UV illumination
446 emphasizes the presence of pigments due to their iron composition. Indeed, iron ions are known to
447 have a quenching effect on the fluorescence signal, including that of uranyl ions (Gaillou *et al.*, 2008;
448 Chen *et al.*, 2011). Thus, pigments appear clearly as no fluorescence zones on UV photographs, which
449 can be an interesting tool for rock art analysis, such as determination of sampling protocol or
450 dermatoglyph analysis.
451
452 Thus, UV methodology appears to be an efficient non-invasive tool for the *in situ* identification of U-
453 opal mineralization. Due to the green fluorescence resulting from UV excitation, it allows rapid *in situ*
454 detection of the opal mineral phase with direct results and very simple and low-cost equipment. As
455 this method has already been applied with success in some caves, rarely calcareous, for the detection
456 of U-silica complex deposits or concretions, as in Castañar Cave (Garcia-Guinea *et al.*, 2013), this
457 study differs in two ways. First, to our knowledge, this method has never been applied to opal
458 detection in a rock art context. Second, we propose *in situ* opal identification based on spectral
459 features for result validation using a portable UV-LIF instrument. This instrument is currently in
460 development and could not yet be taken into the cave, but preliminary tests applied to flakes in the
461 laboratory confirm its ability to detect opal. Finally, opal mineral characterization can also be achieved
462 with high-spatial resolution at the microscopic scale with a laboratory LIF instrument. Spatially high-
463 resolution fluorescence maps can also provide more information on mineral phase repartition,

development and interaction with other organic and mineral phases present on the sample. Thus, the combination of these two methodologies provides a complete solution for the identification and detection of opal mineralization in both sampling and analytical strategies and *in situ* characterization.

### 5.2 What do we know about Points Cave opal

The results obtained with the analyses presented in this paper and with UV methods applied to samples and *in situ* have provided the first information on opal coatings in Points Cave. Indeed, based on SEM analyses of flakes and µ-samples, Points Cave opal is associated with the amorphous opal type (type A). XRD is usually performed for precise opal type determination (Curtis *et al.*, 2019). However, in the case of Points Cave opal, this analysis is difficult to perform due to the opal thin layer on calcareous substrate and iron-rich pigments. Analyses at macro- and microscopic scales suggest thin film deposition as a mineralization type, such as silica skins observed at various rock art sites (Watchman, 1990; Green *et al.*, 2017). This film appears to be deposited under or at the interface with pigment and other crusts. SEM analyses show that the opal structure encapsulates haematite plates on several samples, suggesting strong interactions with pictorial matter (Figure 4). Further studies must be conducted to understand how these two phases interact, but a preliminary hypothesis regarding dissolution and corrosion of haematite plaques by opal can be proposed.

The presence of uranyl ions entrapped in the opal structure was verified by UV spectroscopic analyses. High fluorescence intensities of opal at Points Cave suggest significant content of uranium trapped in the crystalline structure. Similar enrichment in uranium has been found in numerous common opals (Amelin & Black, 2006). However, no quantification of uranium content has yet been realized. Although uranium isotopic measurements were realized on speleothems from Points Cave (stalagmites and coralloids), none was applied on flakes, or flake and wall µ-samples because of their destructive character. According to the literature, as no minerals containing $U^{4+}$ are known to fluoresce, uraniferous silica precipitation involves oxidizing conditions sufficient to mobilize $U^{6+}$ (Zielinski,

1982). For example, Garcia-Guinea *et al.* (2013) explained uranium-bearing opal deposition in Castañar Cave by oxidation of host rocks with meteoritic waters. Zielinski (1982) explained that the initial precipitation of silica was as an amorphous silica gel, with which dissolved uranium coprecipitated before the silica gel dehydrated to form opal. The formation of uranyl-silica complexes is favoured by the natural affinity between aqueous uranyl ions and the silica gel surface, which is very sensitive to pH (optimum range = pH 5-5.5) (Garcia-Guinea *et al.*, 2013).

The *in situ* approach shows an important spread of this coating on Points Cave walls, especially on rock art panels. Concerning the walls a few metres before the rock art panels, the presence of opal needs to be confirmed by spectroscopic measurement and laboratory analyses. Points Cave chronology is constrained by different periods marked by cave wall evolution under climatic and anthropogenic factors (Monney & Jaillet, 2019). The presence of opal mineralization throughout its formation and developmental processes could provide insights into cave chronology. A flaking period was identified subsequent to ornamentation, resulting from mechanical expansion or desquamation, affecting the deepest zones of the cave, and possibly concurrent with gelifraction during MIS2 (Marine Isotope Stage 2) (Monney & Jaillet, 2019). As described previously, UV photographs indicated the absence of a well-developed opal film in the flaking zone, suggesting that opal formation occurred principally before this flaking period. This could also explain why photographs taken on walls between the cave angle and the rock art sectors displayed less marked fluorescence, as this zone presents high flaking rates (Jaillet & Monney, 2018) (Figure 10).

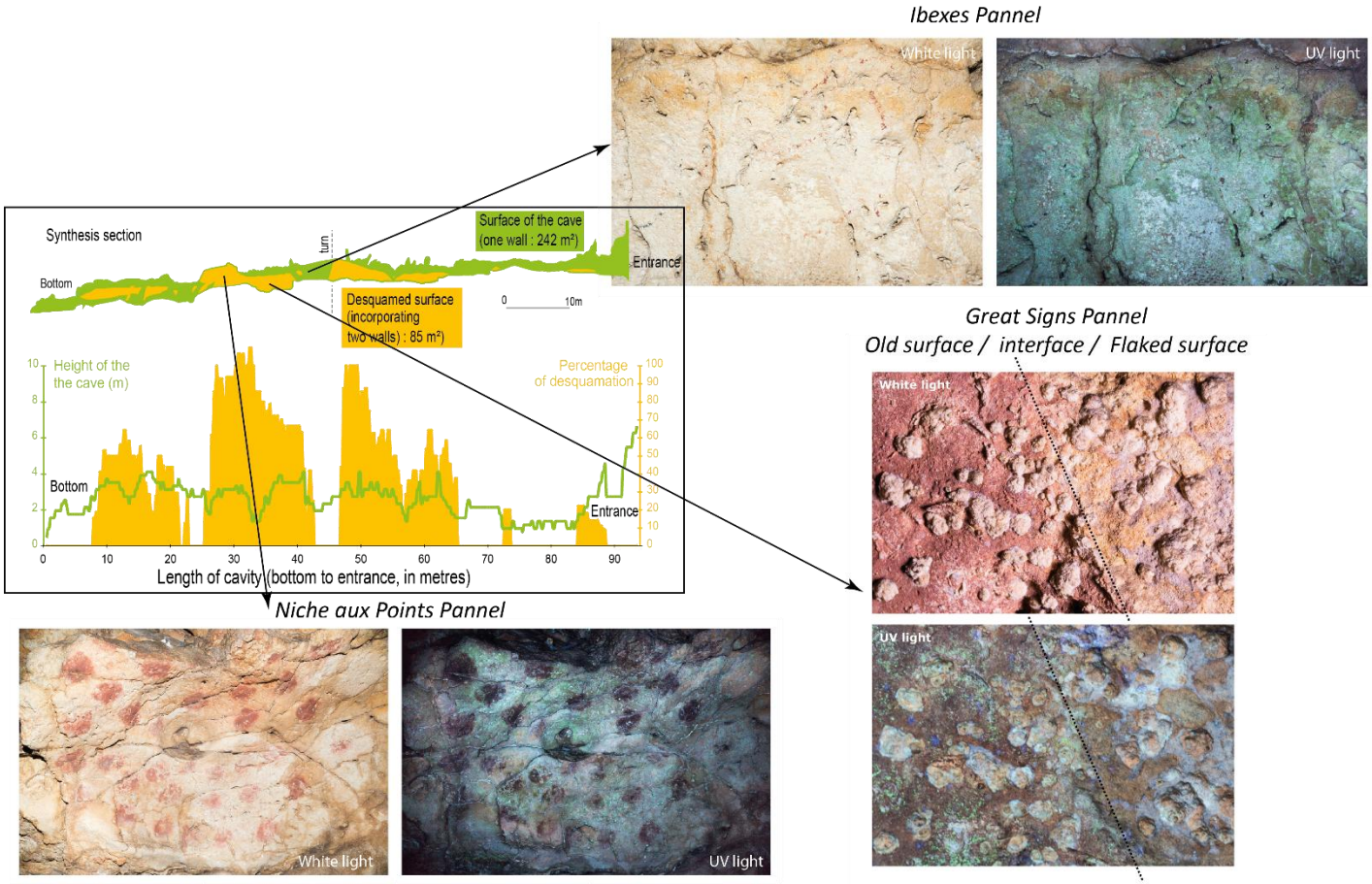


512 ***Figure 10**: Topographic section of Points Cave with estimated flaking and location of white and UV*

513 *light photographs according to Jaillet & Monney, 2018.*

514

515 The chronology of opal deposits over art paintings and drawings cannot be confirmed at this stage.

516 SEM observations show that opal mineralization colonizes empty spaces under, below, and inside

517 pictorial matter. These observations suggest opal postdeposition over painting realization, although

518 prior mineralization cannot be ruled out.

519

520 Thus, ongoing studies are crucial in completing opal coating characterization in Points Cave. This is a

521 tool in understanding cave wall and pigment interactions throughout the factors and processes of opal

522 formation and other mineralization.

523

524 *5.3 Opal factors and formation*

Mineralization origin and formation mechanisms and factors are clues for understanding past climate and cave wall evolution. As this paper presents preliminary results, only hypotheses for opal origin and formation are presented.

Opal, as a hydrated mineral, is associated with fluid circulation. Thus, water is generally involved in precipitation, and silica has to be in solution before precipitation (Chauviré *et al.*, 2017). In Points Cave, the presence of silica coating with high uranium content in the limestone context supports the hypothesis of mineralization originating from groundwater. Wall humidification and water physicochemical properties directly influence the coating formation rate. In very wet sites, the silica skin growth rate can reach 0.25 mm per millennia, whereas occasionally wet sites present a mineralization rate on the order of 0.02 mm per millennia (Aubert *et al.*, 2004). Silica coatings can only be formed and preserved if low infiltration volumes occur, as higher volumes favour dissolution of soluble compounds and decrease silica precipitation (Aubert *et al.*, 2004).

Chauviré *et al.* (2017) explained that even though opal is found in various geological contexts, three main types of formation can be identified: 1) hydrothermal activity, 2) continental weathering and 3) biological precipitation. As no hydrothermal activity was identified at Points Cave, only the latter two types can be involved in opal formation at this site.

Biological formation of opal in caves is less documented than hydrothermal alteration and continental weathering. Various microbial forms and algae have been observed to be associated with opal in caves, such as siliceous algal diatoms (Northup *et al.*, 2001), and are often linked to coralloid concretions. In the case of Points Cave, a few microscopic and cave wall µ-sample observations show undetermined structures containing high carbon content, which could be associated with biological activity. Nevertheless, the hypothesis of biological formation of opal cannot be ruled out or confirmed at this stage, and further studies need to be conducted.

552

553 Continental weathering is defined by rock transformation by meteoric water and a precipitation
554 temperature below 50°C, in contrast to hydrothermal alteration (Chauviré *et al.*, 2017). Silica anions
555 released by this process precipitate because of fluid supersaturation due to various changes in
556 conditions, such as pH or temperature (Devès *et al.*, 2012; Chauviré *et al.*, 2017). Thus,
557 supersaturation of silica solutions may be initiated by a drop in temperature or pH or an increase in
558 salinity. When a solution is supersaturated in SiO2, silicic acid could polymerize to form a colloidal
559 suspension from which amorphous silica can precipitate. Polymerization is controlled by temperature
560 (decreasing T° increases the polymerization rate), degree of supersaturation, salinity and mainly pH
561 (maximum polymerization rate around pH 7.5; minimum polymerization rate under pH 3 and above 9)
562 (Devès *et al.*, 2012). One of the most efficient pH-driven mechanisms for silica precipitation involves
563 acidification of highly alkaline solutions (Zielinski, 1982). Such alkaline conditions are not common,
564 but in the case of calcite-dominant material in sediment, pH could reach this threshold (Karkanas *et*
565 *al.*, 1999). Freezing temperature has also been shown to help supersaturation, polymerization and
566 rapid precipitation of opal, whereas low or moderate temperatures induce slow polymerization
567 (months or years) (Devès *et al.*, 2012). Cryo-segregation is another reported genesis, caused by
568 moisture freezing on cave walls, which concentrates dissolved salts. They precipitate out in the case of
569 supersaturation of the solution (Devès *et al.*, 2012). As opal formation probably occurred between the
570 Upper Palaeolithic and the Last Glacial Maximum and because freezing temperatures have been
571 shown to have modified Points Cave wall topography, a temperature decrease represents a realistic
572 factor for opal formation. However, there is currently a lack of evidence to confirm this hypothesis.

573

574 Silica solutions can originate from 1) superficial cover, 2) host rock, or 3) volcanic ash in a continental
575 weathering context (Devès *et al.*, 2012). Volcanic ash is an interesting hypothesis, as it is assumed to
576 provide high contents of silica and uranium and because the Ardèche region had recent volcanic
577 episodes during the Upper Palaeolithic. Indeed, Nomade *et al.* (2016) dated volcanic eruptions in the
578 Bas-Vivarais region between 29 ± 10 ka and 35 ± 8 ka and suggested that Chauvet rock art, 35 km

579 away, could depict volcanic eruption representations. The current alluvial plain and the lowest former
580 alluvial level (+8 m) deposits contain much basaltic material partly derived from Bas-Vivarais lava,
581 which were subjected to intense erosion and weathering in the alluvium terraces (Genuite *et al.*, 2021).
582 Thus, the location and chronology of the volcanic activity (approximately 45 km from Points Cave)
583 represent an interesting origin hypothesis for both silica and uranium contents in opal. However,
584 determining the origin of uranyl-enriched silica solutions is difficult with our current information.
585 Another hypothesis for silica solution origin can be supported by the presence of a marl layer within
586 the Urgonian limestone, which constitutes the cave environment (Sadier, 2013); or by pebbles
587 originating from the Ardèche River and providing silica by infiltration from the overlaying alluvium
588 terrace or by river deposition (Mocochain *et al.*, 2009; Genuite *et al.*, 2021).
589
590 Thus, understanding the origin and mineralization factors that influence opal formation could provide
591 information on chemical and physical processes occurring on the cave wall surface. According to
592 Green *et al.* (2017), this knowledge is "crucial for targeted sample collection and the application of a
593 range of dating techniques as well as for the development of conservation strategies". Further studies
594 still need to be performed to identify opal origin and formation factors at Points Cave.
595
596 *5.4 Chronology and dating*
597
598 Red pigments used in rock art are difficult to date precisely (Aubert *et al.*, 2007). Thus, several studies
599 have proposed indirect dating methods using associated mineral deposits interlaying pictorial matter to
600 date or to provide chronological constraints on rock paintings (Watchman, 1990; Aubert *et al.*, 2007;
601 Aubert *et al.*, 2017), such as opal coatings.
602
603 Indeed, in the first place, opal coating could help to precise relative chronology thanks to knowledge
604 regarding climatic and environmental factors controlling its mineralization, and to its distribution on
605 walls in comparison to other deposits and archaeological material.

606

607 Amorphous silica skins have been used for radiocarbon analyses based on organic remains trapped by
608 mineralization, such as diatoms or algal matter, on different Australian rock art sites (Watchman,
609 2000; Morwood *et al.*, 2010). However, as silica coatings may contain various organic materials, each
610 presenting a specific radiocarbon signature, dating could result in a mixture of different ages by
611 incorporation of younger or older material (Aubert *et al.*, 2017; Green *et al.*, 2017). In addition, the
612 formation processes of these coatings are not fully understood, requiring great caution when using
613 radiocarbon methods (Aubert *et al.*, 2017). Using compound-specific carbon analyses could
614 potentially avoid this problem (Aubert *et al.*, 2017) but are more difficult to apply to thin deposits,
615 especially in rock art contexts.

616

617 Moreover, opal often contains high uranium contents, which could be used for high-precision dating
618 with methods such as $^{230}$U/Th or U/Pb (Zielinski, 1980; Oster *et al.*, 2017). Because of opal's ability to
619 concentrate uranium from water while rejecting Pb and Th, amorphous silica is an interesting
620 alternative to carbonate minerals (Amelin & Black, 2006). Indeed, $^{230}$Th/U and U/Pb methods have
621 been applied to opal and have provided reliable ages (Neymark & Paces, 2013). They enable
622 chronological constraints or dating hydrogenic subsurface water flow, pedogenesis, and processes
623 such as ore formation deposits (Neymark & Paces, 2013). They also have been applied in the case of
624 paleoclimate reconstruction in silica speleothem studies (Lundberg *et al.*, 2010). Depending on the
625 formation processes, opal coating could thus be used for dating purposes.

626

627 In rock art research, dating of amorphous silica deposits could be used as an age constraint for rock
628 drawing events, depending on the pigments and mineral phase superposition. In their study, Aubert *et*
629 *al.* (2007) performed U-series dating on a 2.5 mm thick calcite coating using the MC-ICPMS
630 technique, allowing high spatial and temporal resolution. Even though only micrograms of samples are
631 needed, authors (Aubert *et al.*, 2007; Aubert *et al.*, 2017) have suggested that for samples with U
632 concentrations > 1 ppm, sampling could be largely reduced, and LIBS techniques could also be

633 applied *in situ* with a 100-200 µm diameter ablation spot. As opal concentrates more U than calcite,
634 these techniques appear to be possible. However, for some authors, the application of uranium series
635 dating to silica skins appears difficult to achieve (Green *et al.*, 2017). Sampling that provides sufficient
636 intact fragments for LA-ICP-MS analysis without damaging rock paintings is one of the main issues
637 regarding this application. The difficulty of performing closed system conditions and replicability tests
638 for evaluating dating reliability has also been highlighted by authors.
639
640 Moreover, methods for opal detection could offer supplemental help before sampling for dating.
641 Indeed, precise targeting of uranium-bearing opal enables identification of pure silica phases in mixed
642 samples, detection of high uranium contents or impurity avoidance. In the case of thin layer deposits,
643 such as coralloids, sampling could decrease dating accuracy when mixing different layers (Devès *et*
644 *al.*, 2012). Tracking the location of opal phases could avoid this issue by spatially constraining
645 sampling.
646
647 *5.5 Implication of opal mineral characterization for conservation of rock art material*
648
649 Taphonomy represents a range of transformations affecting archaeological material that distort
650 archaeological records. Thus, rock paintings have undergone a plurality of transformations impacting
651 pigment longevity, colour (Bednarik, 1994) and identification. The exceptional of Points Cave
652 dermatoglyphs has no comparison with other associated parietal sites in Ardèche and begs the question
653 of opal impact on pigment conservation.
654
655 The association of silica skins composed of opal and pigments has been frequently observed at rock art
656 sites, mainly in open-air sites on sandstone and quartzite substrates in Australia or Canada (Watchman,
657 1990; Aubert *et al.*, 2004; Aubert *et al.*, 2012; Huntley, 2012). Some studies have suggested that
658 pigment binding in silica coatings aids rock art visual preservation (Watchman, 1990), providing a
659 resistant layer to chemical weathering. SEM observations on Points Cave flake and wall µ-samples

indeed suggest a strong interaction between pigments and opal, as mineralization penetrates pigment deposits. If the quality of Points Cave paintings tends to corroborate this hypothesis, exfoliation impacting silica skins observed at some sites should also be mentioned, as it could cause removal of associated pigments (Aubert *et al.*, 2004; Green *et al.*, 2017). Thus, exploiting the observed benefits of silica film deposits for conservation strategies has not yet been proven (Green *et al.*, 2017). Furthermore, it has also been observed at open-air sites that silica skins could reduce the colour tone of paintings and drawings at some locations (Green *et al.*, 2017).

If pigment weathering can be influenced by their own properties by inducing changes in surface area, albedo, light transmissivity or moisture (Huntley, 2012), mineral deposits have been recognized to be important factors in rock art taphonomy (Chalmin *et al.*, 2018). In addition to analytical impacts, knowledge of mineral phases is essential because it informs us regarding the physical and chemical impacts on pictorial matter and whether they favour conservation or degradation effects. Mineral phase characterization is thus an important part of conservation strategies, and adapted identification and analytical methods are needed.

## 6. Conclusion

The methodological development proposed in this paper was motivated by the identification of opal in different contexts: *in situ*, in the laboratory, on centimetric objects and on µ-samples. The aim of this identification is to question the possibility of accessing the specificities of the colouring matter applied on the walls (petrography and geochemistry). Therefore, *in situ* identification of silica coating observed in the laboratory was crucial for further studies on pigment characterization.

The results obtained on flakes and flake µ-samples from Points Cave show that UV LIF is an efficient technique to detect and identify uranyl-silica complexes, even on heterogeneous and complex surfaces.

Although opal coating detection is limited by scale (laser beam) and by the outcropping nature of the deposit, UV LIF spectroscopy offers a rapid and non-invasive tool that can easily be brought to the site and positioned in front of the decorated panels. A photograph of green bright fluorescence emitted by opal was used here as a method of *in situ* detection of this mineral coating. A comparison with the UV LIF method shows a great correspondence between the two methods. The first tests of UV illumination in the cave highlight the need to develop an accurate measurement protocol, especially to homogenize light and colour, and the need to validate the identification using UV spectroscopy. In addition to further methodological development, UV optical technique shows great potential because it successfully detects the presence of opal and its distribution on rock art panels.

Thus, the results obtained with our methodology provide insights into disturbances in the classical *in situ* spectroscopic analyses (pXRF and Raman) observed at Points Cave. The identification and characterization of opal coatings is thus essential because of their impact on *in situ* analysis, which does not allow the detection of iron spectroscopic signal. For this reason, we propose early, on-site observations combined with sampling of surrounding material, such as fallen flakes from cave walls, as an alternative strategy to i) characterize pigment-associated mineral phases, ii) choose the best site-adapted combination of techniques and devices for *in situ* analyses and iii) define laboratory analytical strategies depending on the pictorial matter environment.

Moreover, optical methods with *in situ* visual detection, such as the UV light illumination method proposed in this paper, represent an interesting tool to add to sampling and analytical strategies. Visualization at a larger scale of the presence and distribution of mineral deposits that could interfere with pigment analyses is a great help in locating sampling or *in situ* measurements to avoid interference.

In addition to analytical impacts, the detection and identification of mineral phases can provide valuable information on the pigment environment and human practice chronology. If speleothems are considered an accurate archive for past climate and environment, other mineral deposits could provide

informative records on the setting and evolution of archaeological evidence. Applying a specific methodology for their characterization is thus an efficient tool in improving rock art knowledge.

Thanks to opal mineralization detection utilizing UV methodologies on cave walls, a discussion on its formation and associated factors, such as climatic, hydrologic or geomorphologic conditions over time can be started. Thus, the mineral form described as opal-A can provide elements on cave natural history.


## Acknowledgements

We would like to thank Frédérique Charlot, microscopist at CMTC (INPE, Grenoble). Funding was provided by ANR LabCom SpecSolE, DRAC Occitanie, DRAC AURA (Pigmentothèque project), French Ministry of Culture and University Savoie Mont Blanc.


## Conflict of interest disclosure

The authors declare they have no conflict of interest relating to the content of this article.

## Data, script and code availability

*SEM data:*

https://doi.org/10.6084/m9.figshare.16832593.v2

https://doi.org/10.6084/m9.figshare.16832557.v3

https://doi.org/10.6084/m9.figshare.16832452

https://doi.org/10.6084/m9.figshare.16832605

*Single UV fluorescence measurement (raw data):* https://doi.org/10.6084/m9.figshare.16837180.v1

*UV fluorescence cartography measurement (raw data):*

https://doi.org/10.6084/m9.figshare.16837324.v1

*UV fluorescence data processing (Matlab script):* https://doi.org/10.6084/m9.figshare.16837405.v1

## Bibliography


Amelin, Y., Back, M., 2006. Opal as a U–Pb geochronometer: search for a standard. Chemical Geology 232, 67–86.

Araya, J.A., Carneiro, R.L., Arévalo, C., Freer, J., Castillo, R. del P., 2017. Single pixel quantification strategies using middle infrared hyperspectral imaging of lignocellulosic fibers and MCR-ALS analysis. Microchemical Journal 134, 164–172.

Aubert, M., Brumm, A., Taçon, P.S., 2017. The timing and nature of human colonization of Southeast Asia in the late Pleistocene: A rock art perspective. Current Anthropology 58, S553–S566.

Aubert, M., 2012. A review of rock art dating in the Kimberley, Western Australia. Journal of Archaeological Science 39, 573–577.

Aubert, M., O'Connor, S., McCulloch, M., Mortimer, G., Watchman, A., Richer-LaFlèche, M., 2007. Uranium-series dating rock art in East Timor. Journal of Archaeological Science 34, 991–996.

Aubert, M., Watchman, A., Arsenault, D., Gagnon, L., 2004. L'archéologie rupestre du Bouclier canadien : Potentiel archéométrique. Canadian Journal of Archaeology/Journal Canadien d'Archéologie 51–74.

Barbarand, J., Nouet, J., 2020. Pétrographie et minéralogie des coralloïdes de la grotte au Points, in: Monney J. (Dir.). Projet Datation Grottes Ornées : Rapport d'activité 2020. Grotte Aux Points

765 (Aiguèze). Rapport Non Publié., Ministère de La Culture, SRA Occitanie, Montpellier.
766
767 Bassel, L., 2017. Genèse de faciès calcitiques : mondmilch et coralloïdes. Étude multiphysique des
768 concrétions de la grotte laboratoire de Leye (Dordogne) (Thèse). Université Bordeaux Montaigne.
769
770 Bednarik, R.G., 1994. A taphonomy of palaeoart. Antiquity 68, 68–74.
771
772 Boyko, V., Dovbeshko, G., Fesenko, O., Gorelik, V., Moiseyenko, V., Romanyuk, V., others, 2011.
773 New optical properties of synthetic opals infiltrated by DNA. Molecular Crystals and Liquid Crystals
774 535 (1), 30-41.
775
776 Castro, R.C., Ribeiro, D.S., Santos, J.L., Páscoa, R.N., 2021. Near infrared spectroscopy coupled to
777 MCR-ALS for the identification and quantification of saffron adulterants: Application to complex
778 mixtures. Food Control 123, 107776.
779
780 Chalmin, E., Hoerlé, S.H., Reiche, I., 2018. Taphonomy on the Surface of the Rock Wall. Oxford
781 University Press.
782
783 Chanteraud, C., 2020. Matières colorantes et grottes ornées des gorges de l'Ardèche. Méthodes
784 d'analyse des ressources et liens culturels au Paléolithique supérieur : application à la grotte aux Points
785 (Aiguèze, Gard, France) (Thèse). Université Savoie Mont Blanc.
786
787 Chanteraud, C., Chalmin, E., Hoerlé, S., Salomon, H., Monney, J., 2019. Relation entre les matières
788 colorantes issues des fouilles et des parois ornées. Méthodologie et première perspective comparative
789 à la Grotte aux Points (Aiguèze, Gard, France). Karstologia pp 1-12.
790
791 Chauviré, B., Rondeau, B., Mangold, N., 2017. Near infrared signature of opal and chalcedony as a

792 proxy for their structure and formation conditions. European Journal of Mineralogy 29, 409–421.
793
794 De Juan, A., Jaumot, J., Tauler, R., 2014. Multivariate Curve Resolution (MCR). Solving the mixture
795 analysis problem. Analytical Methods 6, 4964–4976.
796
797 Curtis, N.J., Gascooke, J.R., Johnston, M.R., Pring, A., 2019. A review of the classification of opal
798 with reference to recent new localities. Minerals 9, 299.
799
800 DeNeufville, J., Kasdan, A., Chimenti, R., 1981. Selective detection of uranium by laser-induced
801 fluorescence: a potential remote-sensing technique. 1: Optical characteristics of uranyl geologic
802 targets. Applied Optics 20, 1279–1296.
803
804 Deschamps, E.B., Chauvet, J.M., Hillaire, C., 2018. La grotte aux Points d'Aiguèze : récits de
805 découverte d'une ornementation pariétale. Karstologia 72, 13–14.
806
807 Devès, G., Perroux, A.-S., Bacquart, T., Plaisir, C., Rose, J., Jaillet, S., Ghaleb, B., Ortega, R., Maire,
808 R., 2012. Chemical element imaging for speleothem geochemistry: Application to a uranium-bearing
809 corallite with aragonite diagenesis to opal (Eastern Siberia, Russia). Chemical Geology 294, 190–202.
810
811 Flörke, O., Graetsch, H., Röller, K., Martin, B., Wirth, R., 1991. Nomenclature of micro-and non-
812 crystalline silica minerals. Neues Jahrbuch für Mineralogie, Abhandlungen 163, 19–42.
813
814 Fritsch, E., Megaw, P.K., Spano, T.L., Chauviré, B., Rondeau, B., Gray, M., Hainschwang, T., Renfro,
815 N., 2015. Green-luminescing hyalite opal from Zacatecas, Mexico. J. Gemmol 34, 490–508.
816
817 Fritsch, E., Mihut, L., Baibarac, M., Baltog, I., Ostrooumov, M., Lefrant, S., Wery, J., 2001.
818 Luminescence of oxidized porous silicon: Surface-induced emissions from disordered silica micro-to

819 nanotextures. Journal of Applied Physics 90, 4777–4782.
820
821 Fritsch, E., Wéry, J., Jonusauskas, G., Faulques, E., 2003. Transient photoluminescence from highly
822 disordered silica-rich natural phases with and without nanostructures. Physics and chemistry of
823 minerals 30, 393–400.
824
825 Gaillou, E., Delaunay, A., Rondeau, B., Bouhnik-le-Coz, M., Fritsch, E., Cornen, G., Monnier, C.,
826 2008. The geochemistry of gem opals as evidence of their origin. Ore Geology Reviews 34, 113–126.
827
828 Garcia-Guinea, J., Fernandez-Cortes, A., Alvarez-Gallego, M., García-Antón, E., Casas-Ruiz, M.,
829 Blázquez-Pérez, D., Teijón, O., Cuezva, S., Correcher, V., Sanchez-Moral, S., 2013. Leaching of
830 uranyl–silica complexes from the host metapelite rock favoring high radon activity of subsoil air: case
831 of Castañar cave (Spain). Journal of Radioanalytical and Nuclear Chemistry 298, 1567–1585.
832
833 Gorobets, B., Engoyan, S., Sidorenko, G., 1977. Investigation of uranium and uranium-containing
834 minerals by their luminescence spectra. Soviet Atomic Energy 42, 196–202.
835
836 Green, H., Gleadow, A., Finch, D., Hergt, J., Ouzman, S., 2017. Mineral deposition systems at rock art
837 sites, Kimberley, Northern Australia—Field observations. Journal of Archaeological Science: Reports
838 14, 340–352.
839
840 Huntley, J., 2012. Taphonomy or painT recipe: In situ portable x-ray fluorescence analysis of two
841 anthropomorphic motifs from the Woronora Plateau, New South Wales. Australian Archaeology 75,
842 78–94.
843
844 Huntley, J., Aubert, M., Ross, J., Brand, H. E., Morwood, M. J., 2015. One colour, (at least) two
845 minerals: a study of mulberry rock art pigment and a mulberry pigment ‘quarry’from the Kimberley,

northern Australia. Archaeometry 57 (1), 77-99.

Jaillet, S., Monney, J., 2018. Analyse 3D des volumes et remplissages souterrains de la grotte aux Points au temps des fréquentations paléolithiques (Aiguèze, Gard). Karstologia 72, 27–36.

Jaumot, J., de Juan, A., Tauler, R., 2015. MCR-ALS GUI 2.0: New features and applications. Chemometrics and Intelligent Laboratory Systems 140, 1–12.

Jaumot, J., Gargallo, R., de Juan, A., Tauler, R., 2005. A graphical user-friendly interface for MCR-ALS: a new tool for multivariate curve resolution in MATLAB. Chemometrics and intelligent laboratory systems 76, 101–110.

Karkanas, P., Kyparissi-Apostolika, N., Bar-Yosef, O., Weiner, S., 1999. Mineral assemblages in Theopetra, Greece: a framework for understanding diagenesis in a prehistoric cave. Journal of Archaeological Science 26, 1171–1180.

Kasdan, A., Chimenti, R.J.L., deNeufville, J.P., 1981. Selective detection of uranium by laser-induced fluorescence: a potential remote-sensing technique. 2: Experimental assessment of the remote sensing of uranyl geologic targets. Appl. Opt. 20, 1297–1307.

Kinnunen, K.A., Ikonen, L., 1991. Opal, a new hydromorphic precipitate type from gravel deposits in southern Finland. Bulletin of the Geological Society of Finland 63, 95–104.

Kumar, K., 2018. Application of Genetic Algorithm (GA) Assisted Partial Least Square (PLS) Analysis on Trilinear and Non-trilinear Fluorescence Data Sets to Quantify the Fluorophores in Multifluorophoric Mixtures: Improving Quantification Accuracy of Fluorimetric Estimations of Dilute Aqueous Mixtures. Journal of fluorescence 28, 589–596.

873

874 Mas, S., de Juan, A., Tauler, R., Olivieri, A.C., Escandar, G.M., 2010. Application of chemometric
875 methods to environmental analysis of organic pollutants: a review. Talanta 80, 1052–1067.
876

877 McGarry, S. F., Baker, A., 2000. Organic acid fluorescence: applications to speleothem
878 palaeoenvironmental reconstruction. Quaternary Science Reviews 19(11), 1087-1101.
879

880 Monger, H.C., Kelly, E.F., 2002. Silica minerals. Soil mineralogy with environmental applications 7,
881 611–636.
882

883 Monney, J., 2018. L'art pariétal paléolithique de la grotte aux Points d'Aiguèze: définition d'un
884 dispositif pariétal singulier et discussion de ses implications. Karstologia 72, 45–60.
885

886 Monney, J., 2011. Projet Datation Grottes Ornées : Rapport d'activité 2011. Grotte aux Points
887 (Aiguèze). Rapport non publié, Ministère de la Culture, SRA Occitanie, Montpellier.
888

889 Monney, J., Jaillet, S., 2019. Phases de fréquentations humaines, ornementation pariétale et processus
890 naturels : Mise en place d'un cadre chronologique pour la grotte aux Points d'Aiguèze. Karstologia 72,
891 49–62.
892

893 Morwood, M.J., Walsh, G.L., Watchman, A.L., 2010. AMS radiocarbon ages for beeswax and
894 charcoal pigments in north Kimberley rock art. Rock Art Research: The Journal of the Australian
895 Rock Art Research Association (AURA) 27 (1), 3–8.
896

897 Neymark, L., Paces, J.B., 2013. Ion-probe U–Pb dating of authigenic and detrital opal from Neogene-
898 Quaternary alluvium. Earth and Planetary Science Letters 361, 98–109.
899

Neymark, L.A., Amelin, Y.V., Paces, J.B., 2000. 206Pb–230Th–234U–238U and 207Pb–235U geochronology of Quaternary opal, Yucca Mountain, Nevada. Geochimica et Cosmochimica Acta 64, 2913–2928.

Nomade, S., Genty, D., Sasco, R., Scao, V., Féruglio, V., Baffier, D., Guillou, H., Bourdier, C., Valladas, H., Reigner, E., others, 2016. A 36,000-year-old volcanic eruption depicted in the Chauvet-Pont d'Arc Cave (Ardèche, France)? PloS one 11(1), e0146621.

Northup, K.H., Diana, Lavoie, 2001. Geomicrobiology of caves: a review. Geomicrobiology journal 18, 199–222.

Ospitali, F., Smith, D.C., Lorblanchet, M., 2006. Preliminary investigations by Raman microscopy of prehistoric pigments in the wall-painted cave at Roucadour, Quercy, France. J. Raman Spectroscopy. 37, 1063–1071.

Oster, J.L., Kitajima, K., Valley, J.W., Rogers, B., Maher, K., 2017. An evaluation of paired δ18O and (234U/238U) 0 in opal as a tool for paleoclimate reconstruction in semi-arid environments. Chemical Geology 449, 236–252.

Othmane, G., Allard, T., Vercouter, T., Morin, G., Fayek, M., Calas, G., 2016. Luminescence of uranium-bearing opals: Origin and use as a pH record. Chemical Geology 423, 1–6.

Perrette, Y., Delannoy, J.-J., Bolvin, H., Cordonnier, M., Destombes, J.-L., Zhilinskaya, E.A., Aboukais, A., 2000. Comparative study of a stalagmite sample by stratigraphy, laser induced fluorescence spectroscopy, EPR spectrometry and reflectance imaging. Chemical Geology 162, 221–243.

927 Perrette, Y., Delannoy, J. J., Desmet, M., Lignier, V., Destombes, J. L., 2005. Speleothem organic
928 matter content imaging. The use of a Fluorescence Index to characterise the maximum emission
929 wavelength. Chemical Geology 214 (3-4), 193-208.
930
931 Pons-Branchu, E., Bourrillon, R., Conkey, M.W., Fontugne, M., Fritz, C., Gárate, D., Quiles, A.,
932 Rivero, O., Sauvet, G., Tosello, G., 2014. Uranium-series dating of carbonate formations overlying
933 Paleolithic art: interest and limitations. Bulletin de la Société préhistorique française 211–224.
934
935 Quiers, M., Perrette, Y., Chalmin, E., Fanget, B., Poulenard, J., 2015. Geochemical mapping of
936 organic carbon in stalagmites using liquid-phase and solid-phase fluorescence. Chemical Geology 411,
937 240-247.
938
939 Quiles, A., Fritz, C., Alcaide, M.Á.M., Pons-Branchu, E., Torti, J.L.S., Tosello, G., Valladas, H.,
940 2015. Chronologies croisées (C-14 et U/Th) pour l'étude de l'art préhistorique dans la grotte de Nerja:
941 méthodologie. Presented at the Sobre rocas y huesos: las sociedades prehistóricas y sus
942 manifestaciones plásticas, UCO Press. Editorial de la Universidad de Córdoba, pp. 420–427.
943
944 Sadier, B., 2013. 3D et géomorphologie karstique : La grotte Chauvet et les cavités des Gorges de
945 l'Ardèche (Thèse). Université de Savoie, Le-Bourget-Du-Lac.
946
947 Savitzky, A., Golay, M.J.E., 1964. Smoothing and Differentiation of Data by Simplified Least
948 Squares Procedures. Analytical Chemistry. 36, 1627–1639.
949
950 Shao, Q.-F., Pons-Branchu, E., Zhu, Q.-P., Wang, W., Valladas, H., Fontugne, M., 2017. High
951 precision U/Th dating of the rock paintings at Mt. Huashan, Guangxi, southern China. Quaternary
952 Research 88, 1–13.

953

954 Valladas, H., Pons-Branchu, E., Dumoulin, J.P., Quiles, A., Sanchidrián, J.L., Medina-Alcaide, M.Á.,
955 2017. U/Th and 14 C Crossdating of Parietal Calcite Deposits: Application to Nerja Cave (Andalusia,
956 Spain) and Future Perspectives. Radiocarbon 59, 1955–1967.
957
958 Van Beynen, P., Bourbonniere, R., Ford, D., Schwarcz, H., 2001. Causes of colour and fluorescence in
959 speleothems. Chemical Geology 175 (3-4), 319-341.
960
961 Watchman, A., 2000. A review of the history of dating rock varnishes. Earth-Science Reviews 49,
962 261–277.
963
964 Watchman, A., 1990. What are silica skins and how are they important in rock art conservation?
965 Australian Aboriginal Studies 1, 21–29.
966
967 Zhang, X., Tauler, R., 2013. Application of multivariate curve resolution alternating least squares
968 (MCR-ALS) to remote sensing hyperspectral imaging. Analytica chimica acta 762, 25–38.
969
970 Zielinski, R.A., 1982. Uraniferous opal, Virgin Valley, Nevada: Conditions of formation and
971 implications for uranium exploration. Journal of Geochemical Exploration 16, 197–216.
972
973 Zielinski, R.A., 1980. Uranium in secondary silica; a possible exploration guide. Economic Geology
974 75, 592–602.